

Quantifying and maximizing the information flux in recurrent neural networks

Claus Metzner^{1,2}, Marius E. Yamakou³, Dennis Voelkl¹, Achim Schilling^{1,4}, and
Patrick Krauss^{1,4,5}

¹Neuroscience Lab, University Hospital Erlangen, Germany

²Biophysics Lab, Friedrich-Alexander University Erlangen-Nuremberg, Germany

³Department of Data Science, Friedrich-Alexander University Erlangen-Nuremberg, Germany

⁴Cognitive Computational Neuroscience Group, Friedrich-Alexander University Erlangen-Nuremberg,
Germany

⁵Pattern Recognition Lab, Friedrich-Alexander University Erlangen-Nuremberg, Germany

January 31, 2023

Abstract

Free-running Recurrent Neural Networks (RNNs), especially probabilistic models, generate an ongoing information flux that can be quantified with the mutual information $I[\vec{x}(t), \vec{x}(t+1)]$ between subsequent system states \vec{x} . Although, former studies have shown that I depends on the statistics of the network's connection weights, it is unclear (1) how to maximize I systematically and (2) how to quantify the flux in large systems where computing the mutual information becomes intractable. Here, we address these questions using Boltzmann machines as model systems. We find that in networks with moderately strong connections, the mutual information I is approximately a monotonic transformation of the root-mean-square averaged Pearson correlations between neuron-pairs, a quantity that can be efficiently computed even in large systems. Furthermore, evolutionary maximization of $I[\vec{x}(t), \vec{x}(t+1)]$ reveals a general design principle for the weight matrices enabling the systematic construction of systems with a high spontaneous information flux. Finally, we simultaneously maximize information flux and the mean period length of cyclic attractors in the state space of these dynamical networks. Our results are potentially useful for the construction of RNNs that serve as short-time memories or pattern generators.

1 Introduction

Artificial neural networks form the central part in many current machine learning methods, and in particular deep learning [1] systems have found numerous industrial and scientific applications over the past decades ([2]). The neural networks in machine learning systems are typically structured as stacks of neural layers, and the information is usually passing unidirectionally from the input- to the output layer.

By contrast, Recurrent Neural Networks (RNNs) have feed-back loops among their neuronal connections, so that information can continuously 'circulate' within the system [3]. RNNs are therefore autonomous dynamical systems, in which the neurons show ongoing dynamical activity even without external input, and they can moreover be considered as 'universal approximators' [4]. These and other intriguing properties have stimulated a recent boost in the research field of artificial RNNs, producing both new developments and interesting unsolved problems: Due to their recurrent connectivity, RNNs are ideally suited to process time series data [5], and to store sequential input over time

[6, 7, 8, 9, 10]. For instance, it has been shown that RNNs learn robust representations by dynamically balancing compression and expansion [11]. In particular, a dynamical regime called the 'edge of chaos' at the transition from periodic to chaotic behavior [12] has been extensively studied and demonstrated to be important for computation [13, 14, 15, 16, 17, 18, 19, 20, 21, 22], and short-term memory [23, 24]. Furthermore, numerous studies address the issue of how to control the dynamics of RNNs [25, 26, 27], in particular with external or internal noise [28, 29, 30, 31, 32]. Finally, RNNs have been proposed to be a versatile tool in neuroscience research [33]. In particular, very sparse RNNs, as they occur in the human brain [34], have some remarkable properties [35, 36, 37], like e.g. superior information storage capacities [38].

In previous studies, we systematically analyzed the structural and dynamical properties of very small RNNs, i.e. 3-neuron motifs [39], as well as large RNNs [40]. Furthermore, we investigated resonance phenomena in RNNs. For instance, We discovered 'recurrence resonance' [30], where a suitable amount of added external noise maximizes information flux in the network. In addition, we investigated coherent oscillations [31], and 'import resonance' [41, 32], where noise maximizes information uptake in RNNs.

Here, we focus on the Boltzmann Machine as a simple model of probabilistic RNNs with 'spiking' neurons, in the sense that each neuron is either off or on in any given time step t . The momentary global state of such a network, assuming N neurons, can then be described by a vector $\vec{x}(t) = (x_1^{(t)}, x_2^{(t)}, \dots, x_N^{(t)})$, where each component $x_n^{(t)} \in \{0, 1\}$ is a binary number.

In order to quantify the ongoing information flux in such a system, an important quantity is the Mutual Information (MI) between subsequent global system states, here denoted by $I[\vec{x}(t), \vec{x}(t+1)]$. It can take the minimal value of zero, if the neurons are mutually uncoupled and produce statistically independent and temporally uncorrelated random walks with $p(0) = p(1)$. By contrast, the MI takes on the maximal possible value of N bits, where N is the number of binary neurons, if the next global system state can be perfectly predicted from the present state (deterministic behavior), and if moreover all possible states occur equally often (entropy of states $H = N$). An example of the latter extreme case would be a fully deterministic network that periodically 'counts' through all 2^N possible binary system states in a fixed order, in other words, a 2^N -cycle.

In an actual RNN with N neurons, the MI will have some intermediate value between 0 and N bits, and much can be learned by studying how this state-to-state memory depends on various system parameters. For example, it has been investigated [32] in a simple deterministic RNN model how the information flux depends on the statistical properties of the weight matrix elements w_{ij} , which describe the coupling strength from the output of neuron j to the input of neuron i . It was found that in the two-dimensional parameter space spanned by the density d of non-zero connections and the balance b between excitatory and inhibitory connections, RNNs reproducibly show distinct dynamical phases, such as periodic, chaotic and fix-point attractors. All these dynamical phases are linked to characteristic changes of the information flux, and thus can be detected using the MI between subsequent states.

In order to compute this MI numerically, one first has to estimate the joint probability distribution $p(\vec{x}_t, \vec{x}_{t+1})$ for a pair of subsequent states. Unfortunately, the number of possible state pairs in a N -neuron system is $2^N \times 2^N$, and this exponential growth of state space prevents the computation of the MI for systems much larger than $N \approx 10$. One goal of the present study is therefore to test if the full MI can be approximately replaced by numerically more efficient measures of state-to-state memory, in particular measures based on pair-wise neuron-to-neuron correlations. For the future investigation of RNN phase diagrams, we are not primarily interested in the numerical value of the measure, but mainly in whether it rises or falls as a function of certain system control parameters. For this reason, we test in the following to which extent the alternative measures are monotonic transformations of the full MI.

Furthermore, we use evolutionary optimization to find out which kinds of RNN weight matrices lead to a maximum state-to-state memory, that is, a maximum spontaneous flux of information. Related

to this question, we also test if those fundamentally probabilistic networks can actually produce quasi-deterministic n -cycles with a period length that is comparable to the total number of states 2^N .

2 Methods

Symmetrized Boltzmann Machine (SBM)

In the following, we consider a Boltzmann Machine (BM) with N probabilistic logistic neurons that are fully connected to each other. In order to 'symmetrize' the system, we set all biases to zero and convert the binary neuron states $x \in \{0, 1\}$ to zero-mean states $y \in \{-1, +1\}$ before each network update.

Let neuron j at time step t be in the binary state $x_j^{(t)}$. The zero-mean state is computed as

$$y_j^{(t)} = 2 \cdot x_j^{(t)} - 1. \quad (1)$$

The weighted sum of all input signals to neuron i is given by

$$z_i^{(t)} = \sum_{j=1}^N w_{ij} y_j^{(t)}, \quad (2)$$

where w_{ij} is the real-valued positive or negative connection strength (weight) between the output of neuron j and the input of neuron i . The $N \times N$ -matrix W of all connection strengths is called the weight matrix.

The 'on-probability' $p_i^{(t+1)} = \text{prob}(x_i^{(t+1)} = 1)$ that neuron i will be in the binary 1-state in the next time step is given by a logistic function of the weighted sum:

$$p_i^{(t+1)} = \frac{1}{1 + \exp(-z_i^{(t)})}. \quad (3)$$

All N neurons update simultaneously to their new binary state, and the global system state at time step $t \in \{0, 1, 2, \dots\}$ is denoted as the vector

$$\vec{x}(t) = (x_1^{(t)}, x_2^{(t)}, \dots, x_N^{(t)}). \quad (4)$$

Single-neuron SBM

An SBM with only one neuron is fully described by w_{11} , the self-connection strength.

For $w_{11} = 0$, the weighted sum is zero and the on-probability is $1/2$. The single neuron therefore produces a sequence of statistically independent binary states $x \in \{0, 1\}$ with balanced probabilities $\text{prob}(x=0) = \text{prob}(x=1) = 1/2$. This stochastic Markov process corresponds to an unbiased and uncorrelated random walk.

For $w_{11} \neq 0$, the on- and off-probabilities are still balanced, but now subsequent neuron states are statistically dependent. In particular, a positive self-connection generates a persistent random walk in which the same binary states tend to follow each other (such as 00011100111000011). Analogously, a negative self-connection generates an anti-persistent random walk in which the system tends to flip between the two binary states (such as 10101001011010101). This stochastic Markov process corresponds to an unbiased but correlated random walk.

The degree of state-to-state persistence κ in the single-neuron SBM can be quantified by the conditional probability

$$\kappa = \text{prob}(x^{(t+1)} = 1 \mid x^{(t)} = 1) = \text{prob}(x^{(t+1)} = 0 \mid x^{(t)} = 0), \quad (5)$$

and it is obviously determined by the self-connection strength via

$$\kappa = 1 / (1 + \exp(-w_{11})). \quad (6)$$

Here, $\kappa > 1/2$ (due to $w_{11} > 0$) indicates persistence and $\kappa < 1/2$ (due to $w_{11} < 0$) anti-persistence.

Mutual information and Pearson correlations

Assuming two signal sources U and V that emit discrete states with the joint probability $P(u, v)$, the mutual information (MI) between the two sources is defined as

$$I[u, v] = \sum_u \sum_v P(u, v) \log \left(\frac{P(u, v)}{P(u) \cdot P(v)} \right). \quad (7)$$

This formula is applied in two different ways to compute the MI between successive states of a SBM. One way is to directly compute the MI between the vectorial global states, so that $u \equiv \vec{x}(t)$ and $v \equiv \vec{x}(t+1)$. The resulting quantity is denoted as $I[\vec{x}(t), \vec{x}(t+1)]$, and in a SBM with N neurons it can range between 0 and N bit.

In the other application of 7, we focus on a particular pair of neurons m, n and first compute the MI between the successive binary output values of these two neurons, so that $u \equiv x_m(t)$ and $v \equiv x_n(t+1)$. The resulting quantity is denoted as $I[x_m(t), x_n(t+1)]$, and it can range between 0 and 1 bit.

After repeating this computation for all N^2 pairs of neurons, we aggregate the results to a single number by calculating the root-mean-square average $\text{RMS} \{ I[x_m(t), x_n(t+1)] \}_{mn}$, where

$$\text{RMS} \{ A_{mn} \}_{mn} = \sqrt{\frac{1}{MN} \sum_{m=1}^M \sum_{n=1}^N |A_{mn}|^2}. \quad (8)$$

A simpler way to quantify the state-to-state memory in SBMs is by using linear correlation coefficients. Here too, we focus on particular pairs of neurons m, n and compute their normalized Pearson correlation coefficient

$$C[x_m(t), x_n(t+1)] = \frac{\langle (x_m(t) - \mu_m) \cdot (x_n(t+1) - \mu_n) \rangle_t}{\sigma_m \sigma_n}, \quad (9)$$

where μ_i and σ_i denote the mean and the standard deviation of the neuron states $x_i(t)$. The symbol $\langle a(t) \rangle_t$ denotes the temporal average of a time series $a(t)$. In the cases $\sigma_m = 0$ or $\sigma_n = 0$, the correlation coefficient is set to zero.

The N^2 resulting pairwise correlation coefficients are again aggregated to a single number using the RMS average 8.

Summing up, our three quantitative measures of state-to-state memory are the full mutual information $I[\vec{x}(t), \vec{x}(t+1)]$, the average pair-wise mutual information $\text{RMS} \{ I[x_m(t), x_n(t+1)] \}_{mn}$, and the average pair-wise Pearson correlations $\text{RMS} \{ C[x_m(t), x_n(t+1)] \}_{mn}$.

Numerical calculation of the MI

In a numerical calculation of the full mutual information $I[\vec{x}(t), \vec{x}(t+1)]$, we first generate a sufficiently long time series $\vec{x}(t)$ of SBM states. From this simulated time series, we estimate the joint probability $P(\vec{x}(t), \vec{x}(t+1))$ by counting how often the different combinations of subsequent states occur. Next, we compute from the joint probability the marginal probabilities $P(\vec{x}(t))$ and $P(\vec{x}(t+1))$. Finally we compute the MI using formula 7.

Semi-analytical calculation of the MI

In a semi-analytical calculation of the full mutual information $I[\vec{x}(t), \vec{x}(t+1)]$, we first compute the conditional state transition probabilities $P(\vec{x}(t+1) | \vec{x}(t))$. This can be done analytically, because for each given initial state $\vec{x}(t)$ formula 3 gives the on-probabilities of each neuron in the next time step. Using these on-probabilities, it is straightforward to compute the probability of each possible successive state $\vec{x}(t+1)$.

The conditional state transition probabilities $P(\vec{x}(t+1) | \vec{x}(t))$ define the transition matrix \mathbf{M} of a discrete Markov process. It can therefore be used to numerically compute the stationary probabilities $P(\vec{x})_{fin}$ of the 2^N global system states, which can also be written as a probability vector \vec{p}_{fin} . For this purpose, we start with a uniform distribution $P(\vec{x})_{ini} = 1/2^N$ and then iteratively multiply this probability vector with the Markov transition matrix \mathbf{M} , until the change of $P(\vec{x})$ becomes negligible, that is, until $\vec{p}_{fin}\mathbf{M} \approx \vec{p}_{fin}$.

Once we have the stationary state probabilities $P(\vec{x})_{fin}$, we can compute the joint probability of successive states as $P(\vec{x}(t+1), \vec{x}(t)) = P(\vec{x}(t+1) | \vec{x}(t)) P(\vec{x})_{fin}$. After this, the MI is computed using formula 7.

Weight matrix with limited connection strength

In order to generate a $N \times N$ weight matrix where the modulus of the individual connection strength is restricted to the range $|w_{mn}| < W_{max}$, we first draw the matrix elements independently from a uniform distribution in the range $[0, W_{max}]$. Then each of the N^2 matrix elements is flipped in sign with a probability of 1/2.

Scanning through weight matrix space

Given two $N \times N$ weight matrices \mathbf{A} and \mathbf{B} , we can generate a series of intermediate weight matrices \mathbf{W}_k that interpolate linearly between these endpoints in N^2 -dimensional W-space by defining

$$\mathbf{W}_k = (1-x) \cdot \mathbf{A} + x \cdot \mathbf{B} \quad (10)$$

and increasing the mixing factor x in equidistant steps from zero to one.

In Fig.2, we have first generated a whole set of independent random 'edge' matrices \mathbf{A}_k , all restricted to the same range of connection strength $|A_{mn}| < W_{max}$. Then a linear interpolation was performed between each two subsequent edge matrices, as shown in the sketch on top of panel (a) in Fig.2.

Comparing the Signum-Of-Change (SOC)

Two real-valued functions $f(x)$ and $g(x)$ of a real-valued parameter x are called **monotonic transformations** of each other, if the sign of their derivative is the same for all x in their domain:

$$\text{sgn} \left(\frac{df}{dx}(x) \right) = \text{sgn} \left(\frac{dg}{dx}(x) \right) \quad \forall x. \quad (11)$$

In a plot of $f(x)$ and $g(x)$, the two functions will then always rise and fall simultaneously, albeit to a different degree. Accordingly, possible local maxima and minima will occur at the same x -positions, so that both $f(x)$ and $g(x)$ can be used equally well as objective functions for optimizing x .

In this work, we consider cases where two functions are only approximately monotonic transformations of each other, and our goal is to quantify the degree of this monotonic relation. For this purpose, we numerically evaluate the functions for an arbitrary sequence of M arguments $\{x_1, x_2, \dots, x_M\}$ in the domain of interest, yielding two 'time series' $\{f_1, f_2, \dots\}$ and $\{g_1, g_2, \dots\}$. We then compute the signum of the changes between subsequent function values,

$$S_n^{(f)} = \text{sgn}(f_n - f_{n-1}) \quad \text{and} \quad S_n^{(g)} = \text{sgn}(g_n - g_{n-1}), \quad (12)$$

which yields two discrete series $S_n^{(f,g)} \in \{-1, 0, +1\}$ of length $M-1$. Next, we count the number N_c of corresponding entries, that is, the number of cases where $S_n^{(f)} = S_n^{(g)}$. We finally compute the ratio $r_{SOC} = N_c/(M-1)$, which can range between $r_{SOC}=0$, indicating 'anti-correlated' behavior where minima of $f(x)$ correspond to maxima of $g(x)$, and $r_{SOC}=1$, indicating that the two functions are perfect monotonic transformations of each other. A value $r_{SOC}=0.5$ indicates that the two functions are not at all monotonically related. In the text, we refer to r_{SOC} simply as the 'SOC measure'.

Evolutionary optimization of weight matrices

In order to maximize some objective function $f(\mathbf{W})$ that characterizes the 'fitness' of a weight matrix, we start with a matrix \mathbf{W}_0 in which all elements are zero (The neurons of the corresponding SBM will then produce independent and non-persistent random walks, so that the MI between successive states is zero). The fitness $f_0 = f(\mathbf{W}_0)$ of this starting matrix is computed.

- (0) The algorithm is now initialized with $\mathbf{W} := \mathbf{W}_0$ and $f := f_0$.
- (1) We then generate a mutation of the present weight matrix \mathbf{M} by adding independent random numbers Δw_{mn} to the N^2 matrix elements. In our case we draw these random fluctuations Δw_{mn} from a normal distribution with zero mean and a standard deviation of 0.1. The fitness $f_{mut} = f(\mathbf{W} + \Delta \mathbf{W})$ of the mutant is computed.
- (2) If $f_{mut} > f$, we set $\mathbf{W} := \mathbf{W} + \Delta \mathbf{W}$ and $f := f_{mut}$. Otherwise the last matrix is retained. The algorithm then loops back to (1).

We iterate the evolutionary loop until the fitness does no longer increase significantly.

Visualization with Multi-Dimensional Scaling (MDS)

A frequently used method to generate low-dimensional embeddings of high-dimensional data is t-distributed stochastic neighbor embedding (t-SNE) [42]. However, in t-SNE the resulting low-dimensional projections can be highly dependent on the detailed parameter settings [43], sensitive to noise, and may not preserve, but rather often scramble the global structure in data [44, 45]. In contrast to that, multi-Dimensional-Scaling (MDS) [46, 47, 48, 49] is an efficient embedding technique to visualize high-dimensional point clouds by projecting them onto a 2-dimensional plane. Furthermore, MDS has the decisive advantage that it is parameter-free and all mutual distances of the points are preserved, thereby conserving both the global and local structure of the underlying data.

When interpreting patterns as points in high-dimensional space and dissimilarities between patterns as distances between corresponding points, MDS is an elegant method to visualize high-dimensional data. By color-coding each projected data point of a data set according to its label, the representation of the data can be visualized as a set of point clusters. For instance, MDS has already been applied to visualize for instance word class distributions of different linguistic corpora [50], hidden layer representations (embeddings) of artificial neural networks [51, 52], structure and dynamics of recurrent neural networks [39, 30, 40], or brain activity patterns assessed during e.g. pure tone or speech perception [53, 50], or even during sleep [54, 55, 56]. In all these cases the apparent compactness and mutual overlap of the point clusters permits a qualitative assessment of how well the different classes separate. We use MDS to visualize sets of weight matrices in Fig.4.

Finding the cyclic attractors of a SBM

Given a weight matrix \mathbf{W} , we first calculate analytically the conditional state transition probabilities $P(\vec{x}(t+1) | \vec{x}(t))$. We then find for each possible initial state $\vec{x}(t)$ the subsequent state $\vec{x}(t+1)_{max}$ with the maximal transition probability. We thus obtain a map $\text{SUCC}(\vec{x}(t))$ that yields the most probable successor for each given state.

This map now describes a finite, deterministic, discrete dynamical system. The dynamics of such a system can be described by a 'state flux graph' which has 2^N nodes corresponding to the possible

global states, and links between those nodes that indicate the deterministic state-to-state transitions. Nodes can have self-links (corresponding to 1-cycles = fixed points), but each node can have only one out-going link in a deterministic system. All states (nodes) are either part of a periodic n -cycle, or they are transient states that lead into an n -cycle. Of course, the maximum possible period length is $n_{max} = 2^N$.

In order to find the n -cycles from the successor map, we start with the first system state and follow its path through the state flux graph, until we arrive at a state that was already in that path before (indicating that a complete cycle was run through). We then cut out from this path only the states which are part of the cycle, discarding possible transient states. The cycle is stored in a list.

The same procedure is repeated for all initial system states, and all the resulting cycles are stored in the list. We finally remove from the list all extra copies of cycles that have been stored multiple times. This leads to the complete set of all n -cycles, which can then be further evaluated, for example to compute the individual cycle lengths n or their mean value.

3 Results

Single neuron example

Mutual information (MI) is a very general way to quantify the relatedness of two random variables x and y , because it only depends on the joint probability $P(x, y)$ of the various value combinations and can therefore capture arbitrary non-linear dependencies between the two variables. Indeed, the MI would remain invariant if x and y were replaced by injective functions $f(x)$ and $g(y)$.

By contrast, correlation coefficients are essentially averages of the product $x \cdot y$ of the momentary variable values, and therefore they change when the values x and y are replaced by injective functions of themselves (such as x^3 and y^3). It is also well-known that correlation coefficients can capture only linear relations.

Nevertheless, there are certain special cases where the MI and suitably modified correlation coefficients show a quite similar behavior. As a simple example, we consider a SBM that consists only of a single neuron with self-connection strength w_{11} (Sketch on top of Fig.1). The system produces a random walk of binary (0,1) neuron states that changes from temporally anti-persistent to persistent behavior as w_{11} is tuned from negative to positive values (See times series on top of Fig.1 and Methods for details).

As both anti-persistence and persistence are predictable behaviors, the MI between subsequent states, denoted by $I[x(t), x(t+1)]$ approaches the maximum possible value of 1 bit both in the limit of strongly negative and strongly positive connection weights w_{11} (Fig.1, orange curve). It reaches the minimum possible value of 0 bit exactly for $w_{11}=0$.

We next compute, again as a function of the control parameter w_{11} , the Pearson correlation coefficient between subsequent states, denoted by $C[x(t), x(t+1)]$, and defined in the Methods section. For strongly negative w_{11} , it approaches its lowest possible value of -1, passes through zero for $w_{11}=0$, and finally approaches its highest possible value of +1 for strongly positive w_{11} (Fig.1, blue curve).

It is possible to make the two functions more similar by taking the modulus of the Pearson correlation coefficient, $ABS\{C[x(t), x(t+1)]\}$ which in this case is equivalent to the root-mean-square average $RMS\{C[x(t), x(t+1)]\}$. This RMS-averaged correlation indeed shares with the MI the minimum and the two asymptotic maxima (Fig.1, black dashed curve).

Based on this simple example and several past observations [57, 40, 41, 32], there is legitimate hope that the computationally expensive mutual information I can be replaced by the numerically efficient $RMS\{C\}$, at least in a certain sub-class of systems. It is clear that, when plotted as a function of some control parameter, the two functions will not have exactly the same shape, but they might at least be monotonic transformations of each other, so that local minima and maxima will appear

at the same position on the parameter axis. If such a monotonic relation exists, $RMS\{C\}$ could be used, in particular, as an I -equivalent objective function for the optimization of state-to-state memory in RNNs.

Comparing global MI with pairwise measures

In multi-neuron networks, the momentary system states are vectors $\vec{x}(t)$. In principle, the standard definition of the correlation coefficient can be applied to this case as well (compare e.g. [52]), but it effectively reduces to the mean of pair-wise neuron-to-neuron correlations. To see this, consider the average over products of states, which represents the essence of a correlation coefficient: For vectorial states, the multiplication can be interpreted as a dot product,

$$\langle \vec{x}(t) \cdot \vec{x}(t+1) \rangle_t = \left\langle \sum_{n=1}^N x_n(t) \cdot x_n(t+1) \right\rangle_t = N \cdot \text{MEAN} \{ \langle x_n(t) \cdot x_n(t+1) \rangle_t \}_n, \quad (13)$$

which leads to a mean of single-neuron auto-correlations.

In order to include also cross-correlations between different neurons, the multiplication should better be interpreted as an outer product. Moreover, to make the measure more compatible with the MI, the mean can be replaced by a root-mean-square average. We thus replace

$$\text{MEAN} \{ \langle x_n(t) \cdot x_n(t+1) \rangle_t \}_n \longrightarrow \text{RMS} \{ \langle x_m(t) \cdot x_n(t+1) \rangle_t \}_{mn} \quad (14)$$

More precisely, we use the quantity $\text{RMS} \{ C[x_m(t), x_n(t+1)] \}_{mn}$, an average of normalized cross correlation coefficients, which is defined in the Method section. In a similar way, we also define an average over pair-wise mutual information values, denoted by $\text{RMS} \{ I[x_m(t), x_n(t+1)] \}_{mn}$. We thus arrive at three different measures for the state-to-state memory, which are abbreviated as I , $\text{RMS}\{C\}$ and $\text{RMS}\{I\}$. Our next goal is to test how well these measures match when applied to the spontaneous flux of states in SBMs.

As mentioned before, the best we can expect is that these measures are monotonic transformations of each other and thus share the locations of local maxima and minima as functions of some control parameter. In the previous subsection, we used the matrix element w_{11} as such a tune-able parameter, but in the case of N -neuron networks, all N^2 connection strengths can be tuned, either independently or in arbitrary combinations. To simplify the analysis, we define a continuous path $\mathbf{M}(s)$ through the N^2 -dimensional space of weight matrices (in the following called the 'W-space'), which is parameterized by a real-valued variable s (For details see Method section).

As we move along this path through W-space, the three measures I , $\text{RMS}\{C\}$ and $\text{RMS}\{I\}$ rise and fall, usually to different degrees, but we can count how often the Signum Of Change (abbreviated as SOC and introduced in the Method section) agrees among the three measures. The fraction r_{SOC} of matching SOC values is a quantitative measure for how well the three quantities are monotonically related. For two statistically independent measures, one would expect $r_{SOC} = 0.5$, and $r_{SOC} = 1$ would indicate that the two measures are perfect monotonic transformations of each other.

When generating the path through W-space, we make sure that a sufficient variety of weight matrices is encountered on the way. For this reason, the absolute values of the matrix elements are drawn from a uniform distribution in a suitable range ($|w_{mn}| \in [a, b]$), and their signs are made positive or negative with equal probability.

In a first numerical experiment, we explore networks with moderate connection weights ($|w_{mn}| \in]0, 1[$), a regime that we have already analyzed in some of our former papers on RNN dynamics [40, 32]. Here we find that the maxima and minima of the three measures agree well (Fig.2(a)), and the curves even match in shape after normalizing them to zero mean and unit variance by z-scoring (Fig.2(b)). Indeed, a quantitative test of monotonic relatedness (Fig.2(d)) yields $r_{SOC} = 0.914$ between I and $\text{RMS}\{C\}$, $r_{SOC} = 0.886$ between $\text{RMS}\{I\}$ and $\text{RMS}\{C\}$, and $r_{SOC} = 0.830$ between I

and $\text{RMS}\{I\}$. This result suggests that $\text{RMS}\{C\}$ can be used as a relatively accurate and numerically efficient measure of state-to-state memory, at least in networks with moderately strong connection weights.

However, the situation changes drastically when we move to networks with strong connection weights ($|w_{mn}| \in [1, 5]$), which drive the neurons into the saturation regime of their sigmoid activation functions. A plot of the three measures shows that the two pair-wise measures still agree well with each other, whereas the full MI now behaves in a completely different way (Fig.2(c)). This is also confirmed by the quantitative evaluation (Fig.2(e)), which still yields $r_{SOC} = 0.917$ between $\text{RMS}\{C\}$ and $\text{RMS}\{I\}$, but now $r_{SOC} = 0.315$ between I and $\text{RMS}\{I\}$ and $r_{SOC} = 0.316$ between I and $\text{RMS}\{C\}$. The last two values are well below 0.5 and thus indicate even an 'anti-correlated' behavior between the full MI and the pair-wise measures.

Evolutionary optimization of state-to-state memory

We now turn to our second major research problem of systematically maximizing the spontaneous information flux in free-running SBMs, or in other words, maximizing state-to-state mutual information I . Obviously, a system optimized for this goal must simultaneously have a rich variety of system states (large state entropy H) and be highly predictable from one state to the next (quasi-deterministic behavior). It is however unclear how the connection strengths of the network must be chosen to achieve this goal.

We therefore perform an evolutionary optimization of the weight matrix in order to maximize I , subsequently collect some of the emerging solutions, and finally try to reverse-engineer the resulting weight matrices to extract general design principles. We generate the evolutionary variants simply by adding small random numbers to each of the weight matrix elements w_{mn} (See Methods for details), but we restrict the absolute values of the entries w_{mn} to below 5, in order to avoid extremely deterministic behavior.

We start with a 5×5 weight matrix in which all elements are zero. This corresponds to a set of independent neurons without input and results in $N=5$ uncorrelated random walks (Fig.3(a), state-versus-time plot annotated with $t=0$). The objective function I , consequently, is zero at evolution time step $t=0$ (blue curve).

As the evolutionary optimization proceeds, first, several non-zero matrix elements emerge (inset of Fig.3(a)), but eventually only $N=5$ elements survive, all with large absolute values close to the allowed limit, but with different signs (+ in red, - in blue). During this development, the objective function I is monotonically rising to a final value of about 4.68 (blue curve), which is close to the theoretical maximum of 5. At the final evolution time step $t=1900$, the five neurons show a complex and temporally heterogeneous behavior (state-versus-time plot).

Computing the state transition matrix from the final evolved weight matrix (See Methods for how this is done analytically) reveals that each of the $2^5 = 32$ system states has only one clearly dominating successor state, thus enabling quasi-deterministic behavior (Fig.3(b), left panel). However, a plot focusing on the small weights shows that each state also has a few alternative, low-probability successor states (Fig.3(b), right panel). The latter property makes sure that any overly deterministic behavior, such as being trapped in a n -cycle, is eventually broken. Note also that the dominant entries of the state transition matrix are arranged in a very regular way, which is surprising considering the random optimization process by which the system has been created. Finally, a closer inspection of the dominant successor states reveals that the dynamics of this specific SBN at least contains a few 2-cycles (entries marked by colors) as quasi-stable attractors.

We next compute for our evolved SBN the stationary probability of all 32 system states and find that they all occur about equally often Fig.3(c). Besides the quasi-deterministic behavior, this large variety of states (entropy) represents the second expected property of a system with large state-to-state memory.

We finally repeat the evolutionary optimization with different seeds of the random number generator and thus obtain four additional solutions (Fig.3(d)). Remarkably, they are all constructed according to the same design pattern: There are only $N=5$ large elements in the weight matrix (one for each neuron), which can be of either sign, but which never share a common row or column. Due to the latter property, we call this general design pattern, in analogy to certain chess problems, the 'n-rooks principle'.

Do n-rooks matrices maximize state-to-state memory?

At the end of the evolutionary optimization, the weight matrix contains N large entries, whereas the remaining $N^2 - N$ elements are very small but non-zero. In order to test the relevance of these small background matrix elements, we start with an artificially constructed, perfect n-rooks matrix where all background matrix elements are zero, and then gradually fill the background elements with normally distributed random numbers of increasing standard deviation. We find that I , on average, is decreasing by this perturbation (Fig.4(a,b)). Moreover, it turns out that all perfect n-rooks matrices have the same optimal state-to-state memory, which is 4.710 in the case of the 5-neuron networks. This is another surprising result, since network structures following the n-rooks-principle can be extremely different (The figure insets show both the representation as a matrix and as a network graph), including disconnected neurons with self-interactions (a) and chain-like networks (b).

To further demonstrate that n-rook matrices are local maxima of state-to-state memory, we perform a direct visualization of those matrices as points in N^2 -dimensional W-space, using the method of Multi-Dimensional Scaling (MDS, see Methods for details) and color-coding of their I -values. We first generate ten perfect n-rooks matrices as initial points (red dots in Fig.4(c)) and then iteratively add to their matrix elements independent, normally distributed random numbers with a fixed, small standard deviation. This corresponds to a random walk in W-space, and it leads with high probability away from the initial points. As expected for local maxima, we observe that I tends to decrease during this diffusion process (compare color bar). At the same time, the matrices tend to move away from each other in this two-dimensional, distance-preserving MDS-visualization. This is due to the fact that the initial perfect n-rooks matrices are all part of a N -dimensional sub-manifold of W-space. They are relatively close together, because their non-diagonal matrix elements are zero and thus do not contribute to their Euclidean distance. As the matrices are diffusing out of the sub-manifold, their non-diagonal elements are increasing and so their mutual Euclidean distance is increasing as well.

Pair-wise measures of state-to-state memory in the high- I regime

We have shown above that the pair-wise measures of state-to-state memory only approximate the full MI in the regime of moderate neural connection strengths. Moreover, we found that maximizing I leads naturally to n-rooks matrices with N rather large matrix elements. It is therefore interesting whether the pair-wise measures also fail to approximate the full MI in the specific subset of high- I matrices.

To address this question, we generate a large test set of high- I matrices and a control set of matrices which have the same matrix elements, yet arranged in a way that leads to low I . The test set is made by first creating ten perfect n-rooks matrices. We then generate close variants of these ideal matrices by adding sufficiently small random numbers to the matrix elements, leading to narrow clusters around each ideal matrix (dark red spots in Fig.4(d)). The low- I control set is generated from the high- I test set by randomly shuffling the N large 'rook matrix elements' to new positions within the matrix (weak red and weak blue spots in Fig.4(d)).

We find again a reasonable agreement of $SOC = 0.757$ between the pairwise measures $RMS\{I\}$ and $RMS\{C\}$ in the low- I control set (Fig.4(e)), but this agreement is lost in the high- I test set (Fig.4(f)). Surprisingly, the pairwise $RMS\{I\}$ approximates the full I with $SOC = 0.744$ in this

high-MI regime.

Maximizing the cycle length of periodic attractors

It is important to remember that the n-rooks matrices are optima of state-to-state memory under the constraint of a limited magnitude of connection weights (In our case, the limit was set to $|w_{mn}| < 5$). Due to this constraint, the value of $I = 4.710$ achieved in 5-neuron networks is large, but still below the theoretical maximum of $I = 5$.

As already pointed out in the introduction, this theoretical maximum could be realized in a N -neuron system only if it would run deterministically through a 2^N -cycle. It is however not clear if this is actually possible with a SBM. We therefore now turn to the problem of maximizing the cycle length evolutionary.

In order to quantify the cycle length for a given weight matrix, we first compute analytically the state transition matrix. By considering only the most probable successor for each of the 2^N states, we obtain a perfectly deterministic flux of states, which corresponds to a directed graph with only one out-link per node (see Fig.5(d) for some examples). It is straightforward to find all n-cycles in this graph, finally yielding the mean cycle length MCL of the given weight matrix (See Methods for details).

When the mean cycle length is maximized evolutionary, we obtain top values of up to MCL=18 in a 5-neuron system (corresponding to a single 18-cycle with many transient states leading into it). However, the resulting weight matrices are densely populated with relatively small matrix elements (data not shown), and thus each state has multiple successors with comparable transition probabilities. In other words, the optimization has only produced a quasi-stable 18-cycle with a rather short lifetime. It is therefore necessary to not only maximize the mean cycle length MCL, but to simultaneously make sure the system behaves deterministic to a large degree.

We therefore choose as a new objective function the product of the state-to-state memory I and the mean cycle length MCL. Here we find that, at least over sufficiently many time steps, it is indeed possible to maximize both quantities in parallel (Fig.5(a)). For example, one evolutionary run produces a matrix with $I = 4.042$ and MCL=24 (left figure column), another run yields $I = 4.138$ and MCL=20 (right figure column). Due to the now incomplete optimization of I , the resulting weight matrices deviate from the n-rooks principle (See insets of Fig.5(a) and their network representations Fig.5(b)). Correspondingly, the state transition matrices have more than one non-zero entries in each row, however each state has now one clearly dominating successor, leading to a relatively long lifetime of the periodic attractor.

4 Conclusions

This work was focused on the spontaneous flux of information in RNNs, a quantity that we call state-to-state memory and which can be accurately quantified by the mutual information between subsequent global system states. Using a Symmetrized Boltzmann Machine (SBM) as a model system, we have demonstrated that the full mutual information I behaves approximately like a monotonic transformation of the numerically more efficient pair-wise measures $RMS\{C\}$ and $RMS\{I\}$, as long as all connection weights between the RNN neurons are sufficiently small in magnitude. However, even the existence of a few large matrix elements (as in Fig.4(e)), which drive the receiving neurons deeply into the non-linear saturation regime of their activation functions, can lead to higher-order correlations between subsequent states and thus may cause a breakdown of this monotonic relation.

While the theoretical maximum of state-to-state memory I would correspond to a system which cycles deterministically through a single periodic attractor that comprises all 2^N possible states, we could not realize this extreme case with our SBM. Instead, evolutionary maximization of I , combined with a limited magnitude of the neural connections to avoid overly deterministic behavior, led to

weight matrices that are built according the 'n-rooks principle': There are only N dominating negative or positive matrix elements, and their large magnitude creates a quasi-deterministic behavior. These dominating elements are arranged so that they do not have any rows or columns in common. Remarkably, all these perfect n-rooks systems have the same locally optimal I value, and filling up the $N-1$ background matrix elements with non-zero values only degrades the state-to-state memory.

The n-rooks principle is equivalent to the following two conditions: (1) Each row r of the weight matrix, which describes the input strengths of neuron r , has only one dominant entry, and (2) the column position of this dominant entry is different in each row. Condition (1) means that each neuron receives input from only one supplier neuron, and so these networks obey a 'single supplier rule'. Condition (2) implies that there are no two neurons which receive input from the same supplier neuron. Because there are n neurons in total, it follows that each of them is feeding its output to only one unique consumer neuron, corresponding to a 'single consumer rule'. Together, the two rules imply that the system is structured as a set of linear strings of neurons. Since each neuron definitely has a consumer (that is, within the weight matrix it appears in the input row of some other neuron), these strings do not end and so they must be closed loops. Consequently, the n-rooks weight matrix corresponds to a set of closed neuron loops. There can be just one huge loop as in Fig.4(b), n self-loops as in Fig.4(a), or everything in between as in Fig.3(b).

What is the dynamical significance of closed neuron loops? – In a closed loop of m neurons with only positive large connections in between, an initial bit pattern would simply circulate around, creating a trivial m -cycle of states within this m -neuron subspace. But also with mixed negative and positive connections, closed neuron loops create cyclic attractors in their subspace.

What is the dynamical significance of the 'single supplier rule'? – To understand this, let us violate the condition (1) and assume that neuron 1 is receiving inputs both from neuron 2 and neuron 3, and that both input weights are large and positive. Then neuron 1 will be in the on-state at the next time step $t+1$ if either neuron 2, or neuron 3, or both were in the on-state at time t . This would make it possible that different global system states lead into the same global successor state: In the graph of global system states, there would then be several edges converging onto the same successor state (as it typically happens with transient states that all feed the same cyclic attractor). But such a 'convergence of global states' necessarily forces the system into a smaller subset of available states (Note that divergence is not allowed in a deterministic system) and thus reduces the entropy.

This entropy-reducing convergence of global states cannot happen in a system that obeys the 'single supplier rule'. Therefore, n-rooks weight matrices prevent the convergence of global states. In particular, they prevent transient states: All global states are used up as parts of cyclic attractors. In summary, n-rooks weight matrices correspond to sets of closed linear neuron loops, each creating a cyclic dynamical attractor, without any transient states.

5 Discussion

Very large systems, i.e. with a large number of neurons n , constructed according to the n-rooks principle would have a vanishingly small density of non-zero connections, given by $d = N/N^2 = 1/N \rightarrow 0$. Interestingly, we found in one of our former studies on deterministic RNNs a highly unusual behavior at the very edge of the density-balance phase diagram, precisely in the regime that corresponds to these extremely sparsely connected networks [32]. It might therefore be worthwhile to study this low-density regime more comprehensively in future work, considering that the brain also has a very low connection density [34, 58, 59].

We have finally investigated the lengths of the periodic attractors in our SBMs, quantified by the Mean Cycle Lengths (MCL). It turns out that n-rooks networks, against our original expectations, do not have unusually large MCL values (data not shown). In fact, the system in Fig.4(a), consisting of five isolated neurons with self-connections, provides an extreme example where $I = 4.710$ is maximal but $MCL=1$ is minimal. In this system, each neuron is simply generating its own persistent random

walk, iteratively copying its present state into the future. By this way, each of the 2^N global states becomes a fixed point (1-cycle) of the dynamics. Yet, these fixed points are quasi-stable and they occasionally switch among each other, whenever one of the neurons breaks its persistence. When additionally connected to some input connections, such a system would be ideally suited as a short time memory.

However, it is actually not very difficult to achieve relatively long n-cycles in SBMs. Even in a system with random (non-optimized) weight matrix, the MCL is expected to be larger than one. To see this, remember that we first determine for each state the most probable successor and thereby turn the system into a deterministic machine. The probability that the successor of a given state will be the same state (corresponding to a 1-cycle) is only $1/N$, so it is relatively probable that the resulting MCL will be larger than one, particularly in large systems. However, even if a random SBM can have a large MCL, this does not mean much in practice because there will be many possible successors for each momentary state, thus leading to a very short lifetime of the n-cycles.

Finally, we have evolutionary maximized the MCL and run exactly into this problem of long but dynamically unstable cycles. For this reason, we changed the objective function of the evolutionary optimization to the product of state-to-state memory I and the MCL. This led to weight matrices that deviate from the strict n-rooks principle, but which combine large cycle lengths of up to 24 (in a 5-neuron system with only 32 possible global system states in total) with a relatively good dynamic stability of this periodic attractor.

The resulting networks could correspond to the so-called central pattern generators [60] in the brain, which exhibit robust periodic behavior in the absence of input. Within larger neural networks, these types of sub-networks may serve to generate and control periodic movements such as walking, swimming, or flying, and they could also provide time stamps for ordering episodic memory content.

Acknowledgements

This work was funded by the Deutsche Forschungsgemeinschaft (DFG, German Research Foundation) with the grants KR 5148/2-1 (project number 436456810), KR 5148/3-1 (project number 510395418) and GRK 2839 (project number 468527017) to PK, as well as grant SCHI 1482/3-1 (project number 451810794) to AS.

Author contributions

The study was conceived, designed and supervised by CM and PK. Numerical experiments were performed by CM and DV. Results were discussed and interpreted by CM, MY, AS and PK. The paper was written by CM and PK. All authors have critically read the manuscript before submission.

Additional information

Competing financial interests The authors declare no competing interests.

Data availability statement Data and analysis programs will be made available upon reasonable request.

References

- [1] Yann LeCun, Yoshua Bengio, and Geoffrey Hinton. Deep learning. *nature*, 521(7553):436–444, 2015.
- [2] Laith Alzubaidi, Jinglan Zhang, Amjad J Humaidi, Ayad Al-Dujaili, Ye Duan, Omran Al-Shamma, José Santamaría, Mohammed A Fadhel, Muthana Al-Amidie, and Laith Farhan. Review of deep learning: Concepts, cnn architectures, challenges, applications, future directions. *Journal of big Data*, 8(1):1–74, 2021.
- [3] Niru Maheswaranathan, Alex H Williams, Matthew D Golub, Surya Ganguli, and David Sussillo. Universality and individuality in neural dynamics across large populations of recurrent networks. *Advances in neural information processing systems*, 2019:15629, 2019.
- [4] Anton Maximilian Schäfer and Hans Georg Zimmermann. Recurrent neural networks are universal approximators. In *International Conference on Artificial Neural Networks*, pages 632–640. Springer, 2006.
- [5] Herbert Jaeger. The “echo state” approach to analysing and training recurrent neural networks—with an erratum note. *Bonn, Germany: German National Research Center for Information Technology GMD Technical Report*, 148(34):13, 2001.
- [6] Jannis Schuecker, Sven Goedeke, and Moritz Helias. Optimal sequence memory in driven random networks. *Physical Review X*, 8(4):041029, 2018.
- [7] Lars Büssing, Benjamin Schrauwen, and Robert Legenstein. Connectivity, dynamics, and memory in reservoir computing with binary and analog neurons. *Neural computation*, 22(5):1272–1311, 2010.
- [8] Joni Dambre, David Verstraeten, Benjamin Schrauwen, and Serge Massar. Information processing capacity of dynamical systems. *Scientific reports*, 2(1):1–7, 2012.

- [9] Edward Wallace, Hamid Reza Maei, and Peter E Latham. Randomly connected networks have short temporal memory. *Neural computation*, 25(6):1408–1439, 2013.
- [10] Lukas Gonon and Juan-Pablo Ortega. Fading memory echo state networks are universal. *Neural Networks*, 138:10–13, 2021.
- [11] Matthew Farrell, Stefano Recanatesi, Timothy Moore, Guillaume Lajoie, and Eric Shea-Brown. Recurrent neural networks learn robust representations by dynamically balancing compression and expansion. *bioRxiv*, page 564476, 2019.
- [12] Jonathan Kadmon and Haim Sompolinsky. Transition to chaos in random neuronal networks. *Physical Review X*, 5(4):041030, 2015.
- [13] X Rosalind Wang, Joseph T Lizier, and Mikhail Prokopenko. Fisher information at the edge of chaos in random boolean networks. *Artificial life*, 17(4):315–329, 2011.
- [14] Joschka Boedecker, Oliver Obst, Joseph T Lizier, N Michael Mayer, and Minoru Asada. Information processing in echo state networks at the edge of chaos. *Theory in Biosciences*, 131(3):205–213, 2012.
- [15] Chris G Langton. Computation at the edge of chaos: Phase transitions and emergent computation. *Physica D: Nonlinear Phenomena*, 42(1-3):12–37, 1990.
- [16] Thomas Natschläger, Nils Bertschinger, and Robert Legenstein. At the edge of chaos: Real-time computations and self-organized criticality in recurrent neural networks. *Advances in neural information processing systems*, 17:145–152, 2005.
- [17] Robert Legenstein and Wolfgang Maass. Edge of chaos and prediction of computational performance for neural circuit models. *Neural networks*, 20(3):323–334, 2007.
- [18] Nils Bertschinger and Thomas Natschläger. Real-time computation at the edge of chaos in recurrent neural networks. *Neural computation*, 16(7):1413–1436, 2004.
- [19] Benjamin Schrauwen, Lars Buesing, and Robert Legenstein. On computational power and the order-chaos phase transition in reservoir computing. In *22nd Annual conference on Neural Information Processing Systems (NIPS 2008)*, volume 21, pages 1425–1432. NIPS Foundation, 2009.
- [20] Taro Toyoizumi and LF Abbott. Beyond the edge of chaos: Amplification and temporal integration by recurrent networks in the chaotic regime. *Physical Review E*, 84(5):051908, 2011.
- [21] Kuniyiko Kaneko and Junji Suzuki. Evolution to the edge of chaos in an imitation game. In *Artificial life III*. Citeseer, 1994.
- [22] Ricard V Solé and Octavio Miramontes. Information at the edge of chaos in fluid neural networks. *Physica D: Nonlinear Phenomena*, 80(1-2):171–180, 1995.
- [23] Taichi Haruna and Kohei Nakajima. Optimal short-term memory before the edge of chaos in driven random recurrent networks. *Physical Review E*, 100(6):062312, 2019.
- [24] Kohei Ichikawa and Kuniyiko Kaneko. Short term memory by transient oscillatory dynamics in recurrent neural networks. *arXiv preprint arXiv:2010.15308*, 2020.
- [25] Kanaka Rajan, LF Abbott, and Haim Sompolinsky. Stimulus-dependent suppression of chaos in recurrent neural networks. *Physical Review E*, 82(1):011903, 2010.
- [26] Herbert Jaeger. Controlling recurrent neural networks by conceptors. *arXiv preprint arXiv:1403.3369*, 2014.

- [27] Doron Haviv, Alexander Rivkind, and Omri Barak. Understanding and controlling memory in recurrent neural networks. In *International Conference on Machine Learning*, pages 2663–2671. PMLR, 2019.
- [28] Lutz Molgedey, J Schuchhardt, and Heinz G Schuster. Suppressing chaos in neural networks by noise. *Physical review letters*, 69(26):3717, 1992.
- [29] Shuhei Ikemoto, Fabio DallaLibera, and Koh Hosoda. Noise-modulated neural networks as an application of stochastic resonance. *Neurocomputing*, 277:29–37, 2018.
- [30] Patrick Krauss, Karin Prebeck, Achim Schilling, and Claus Metzner. Recurrence resonance” in three-neuron motifs. *Frontiers in computational neuroscience*, 13, 2019.
- [31] Florian Bönsel, Patrick Krauss, Claus Metzner, and Marius E Yamakou. Control of noise-induced coherent oscillations in time-delayed neural motifs. *arXiv preprint arXiv:2106.11361*, 2021.
- [32] Claus Metzner and Patrick Krauss. Dynamics and information import in recurrent neural networks. *Frontiers in Computational Neuroscience*, 16, 2022.
- [33] Omri Barak. Recurrent neural networks as versatile tools of neuroscience research. *Current opinion in neurobiology*, 46:1–6, 2017.
- [34] Sen Song, Per Jesper Sjöström, Markus Reigl, Sacha Nelson, and Dmitri B Chklovskii. Highly nonrandom features of synaptic connectivity in local cortical circuits. *PLoS biology*, 3(3):e68, 2005.
- [35] Sharan Narang, Erich Elsen, Gregory Diamos, and Shubho Sengupta. Exploring sparsity in recurrent neural networks. *arXiv preprint arXiv:1704.05119*, 2017.
- [36] Richard C Gerum, André Erpenbeck, Patrick Krauss, and Achim Schilling. Sparsity through evolutionary pruning prevents neuronal networks from overfitting. *Neural Networks*, 128:305–312, 2020.
- [37] Viola Folli, Giorgio Gosti, Marco Leonetti, and Giancarlo Ruocco. Effect of dilution in asymmetric recurrent neural networks. *Neural Networks*, 104:50–59, 2018.
- [38] Nicolas Brunel. Is cortical connectivity optimized for storing information? *Nature neuroscience*, 19(5):749–755, 2016.
- [39] Patrick Krauss, Alexandra Zankl, Achim Schilling, Holger Schulze, and Claus Metzner. Analysis of structure and dynamics in three-neuron motifs. *Frontiers in Computational Neuroscience*, 13:5, 2019.
- [40] Patrick Krauss, Marc Schuster, Verena Dietrich, Achim Schilling, Holger Schulze, and Claus Metzner. Weight statistics controls dynamics in recurrent neural networks. *PloS one*, 14(4):e0214541, 2019.
- [41] Claus Metzner and Patrick Krauss. Dynamical phases and resonance phenomena in information-processing recurrent neural networks. *arXiv preprint arXiv:2108.02545*, 2021.
- [42] Laurens Van der Maaten and Geoffrey Hinton. Visualizing data using t-sne. *Journal of machine learning research*, 9(11), 2008.
- [43] Martin Wattenberg, Fernanda Viégas, and Ian Johnson. How to use t-sne effectively. *Distill*, 1(10):e2, 2016.
- [44] Catalina A Vallejos. Exploring a world of a thousand dimensions. *Nature biotechnology*, 37(12):1423–1424, 2019.

- [45] Kevin R Moon, David van Dijk, Zheng Wang, Scott Gigante, Daniel B Burkhardt, William S Chen, Kristina Yim, Antonia van den Elzen, Matthew J Hirn, Ronald R Coifman, et al. Visualizing structure and transitions in high-dimensional biological data. *Nature biotechnology*, 37(12):1482–1492, 2019.
- [46] Warren S Torgerson. Multidimensional scaling: I. theory and method. *Psychometrika*, 17(4):401–419, 1952.
- [47] Joseph B Kruskal. Nonmetric multidimensional scaling: a numerical method. *Psychometrika*, 29(2):115–129, 1964.
- [48] Joseph B Kruskal. *Multidimensional scaling*. Number 11. Sage, 1978.
- [49] Michael AA Cox and Trevor F Cox. Multidimensional scaling. In *Handbook of data visualization*, pages 315–347. Springer, 2008.
- [50] Achim Schilling, Rosario Tomasello, Malte R Henningsen-Schomers, Alexandra Zankl, Kishore Surendra, Martin Haller, Valerie Karl, Peter Uhrig, Andreas Maier, and Patrick Krauss. Analysis of continuous neuronal activity evoked by natural speech with computational corpus linguistics methods. *Language, Cognition and Neuroscience*, 36(2):167–186, 2021.
- [51] Achim Schilling, Andreas Maier, Richard Gerum, Claus Metzner, and Patrick Krauss. Quantifying the separability of data classes in neural networks. *Neural Networks*, 139:278–293, 2021.
- [52] Patrick Krauss, Claus Metzner, Nidhi Joshi, Holger Schulze, Maximilian Traxdorf, Andreas Maier, and Achim Schilling. Analysis and visualization of sleep stages based on deep neural networks. *Neurobiology of sleep and circadian rhythms*, 10:100064, 2021.
- [53] Patrick Krauss, Claus Metzner, Achim Schilling, Konstantin Tziridis, Maximilian Traxdorf, Andreas Wollbrink, Stefan Rampp, Christo Pantev, and Holger Schulze. A statistical method for analyzing and comparing spatiotemporal cortical activation patterns. *Scientific reports*, 8(1):1–9, 2018.
- [54] Patrick Krauss, Achim Schilling, Judith Bauer, Konstantin Tziridis, Claus Metzner, Holger Schulze, and Maximilian Traxdorf. Analysis of multichannel eeg patterns during human sleep: a novel approach. *Frontiers in human neuroscience*, 12:121, 2018.
- [55] Maximilian Traxdorf, Patrick Krauss, Achim Schilling, Holger Schulze, and Konstantin Tziridis. Microstructure of cortical activity during sleep reflects respiratory events and state of daytime vigilance. *Somnologie*, 23(2):72–79, 2019.
- [56] Claus Metzner, Achim Schilling, Maximilian Traxdorf, Holger Schulze, Konstantin Tziridis, and Patrick Krauss. Extracting continuous sleep depth from eeg data without machine learning. *arXiv preprint arXiv:2301.06755*, 2023.
- [57] Patrick Krauss, Claus Metzner, Achim Schilling, Christian Schütz, Konstantin Tziridis, Ben Fabry, and Holger Schulze. Adaptive stochastic resonance for unknown and variable input signals. *Scientific reports*, 7(1):1–8, 2017.
- [58] Olaf Sporns. The non-random brain: efficiency, economy, and complex dynamics. *Frontiers in computational neuroscience*, 5:5, 2011.
- [59] Daniel Miner and Jochen Triesch. Plasticity-driven self-organization under topological constraints accounts for non-random features of cortical synaptic wiring. *PLoS computational biology*, 12(2):e1004759, 2016.
- [60] U Bässler. On the definition of central pattern generator and its sensory control. *Biological cybernetics*, 54(1):65–69, 1986.

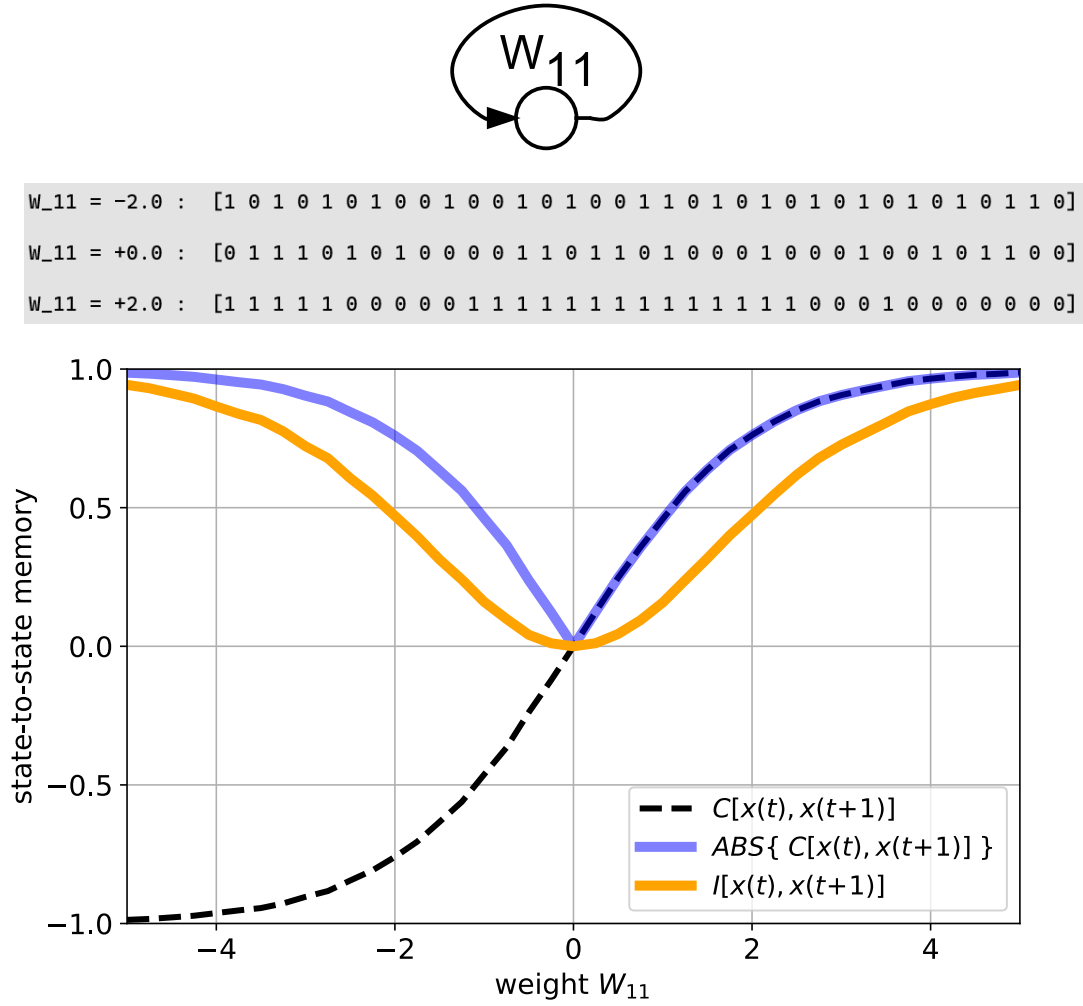


Figure 1: **Mutual information and correlation in a single-neuron SBM.** A symmetrized Boltzmann machine with only one neuron is defined by the self-interaction weight W_{11} (sketch at the top). The binary output series of the system is anti-persistent for $W_{11} < 0$, non-persistent for $W_{11} = 0$ and persistent for $W_{11} > 0$ (printed example sequences on gray background). The mutual information between subsequent system states $I[x(t), x(t+1)]$ (orange curve) is close to its maximal possible value of one for $W_{11} = -5$. As the weight is increased, the MI falls and reaches the minimal possible value of zero for $W_{11} = 0$. It then raises again towards the maximum in a symmetric way. By contrast, the Pearson correlation coefficient between subsequent system states $C[x(t), x(t+1)]$ (dashed black curve) is monotonically increasing from about -1, over zero, to about +1. However, the absolute value of the correlation $|C[x(t), x(t+1)]|$ (blue curve) resembles the mutual information in that it shares the asymptotic limits and the minimum. Note that the absolute value is equivalent to the RMS average in this one-neuron system.

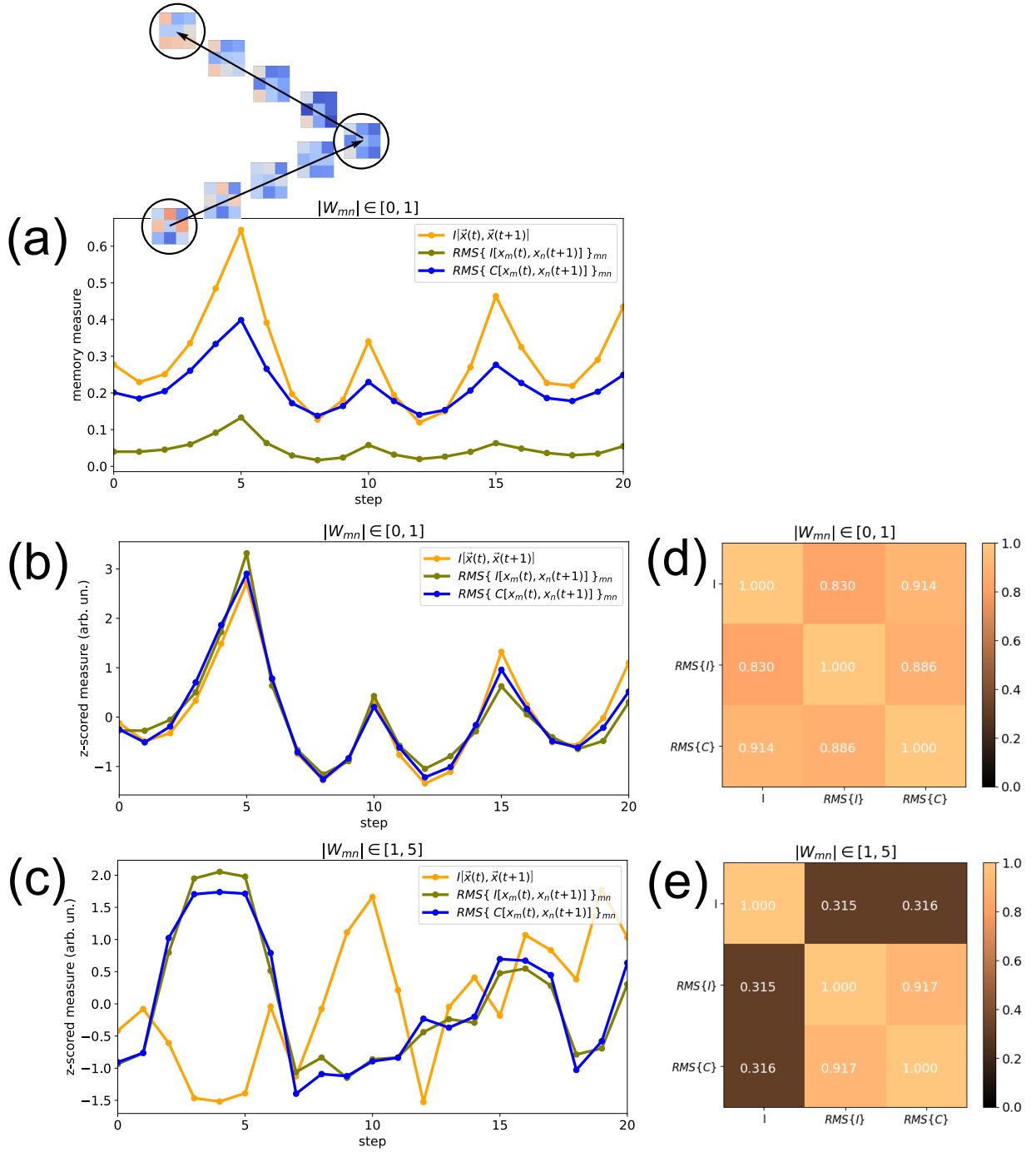


Figure 2: Comparing measures of state-to-state memory in three-neuron SBMs. We generate a series of random weight matrices W that form a continuous path through W -space (sketch on top of panel (a), see Methods for details). For each matrix, we compute the full mutual information $I[\vec{x}(t), \vec{x}(t+1)]$ (orange), the RMS-average of the pairwise mutual information $RMS\{I[x_m(t), x_n(t+1)]\}_{mn}$ (olive), and the RMS-average of the pairwise Pearson correlation $RMS\{C[x_m(t), x_n(t+1)]\}_{mn}$ (blue). **(a)** In the regime of moderate connection weights, with the modulus of weight matrix elements drawn uniformly from the range $|W_{mn}| \in [0, 1]$, we find good agreement of the maxima and minima for all three measures. **(b)** For better comparison, we normalize all measures to zero mean and unit variance (z-scoring). **(c)** In the regime of large connection weights, with the modulus of weight matrix elements drawn uniformly from the range $|W_{mn}| \in [1, 5]$, the two pairwise measures still show a relatively good agreement, but the full mutual information behaves very differently. **(d,e)** We confirm this finding by also computing the three measures for 1000 statistically independent weight matrices. The similarity between the measures is then evaluated with the Signum Of Change (SOC, see Methods for the detailed definition) and presented as heat maps.

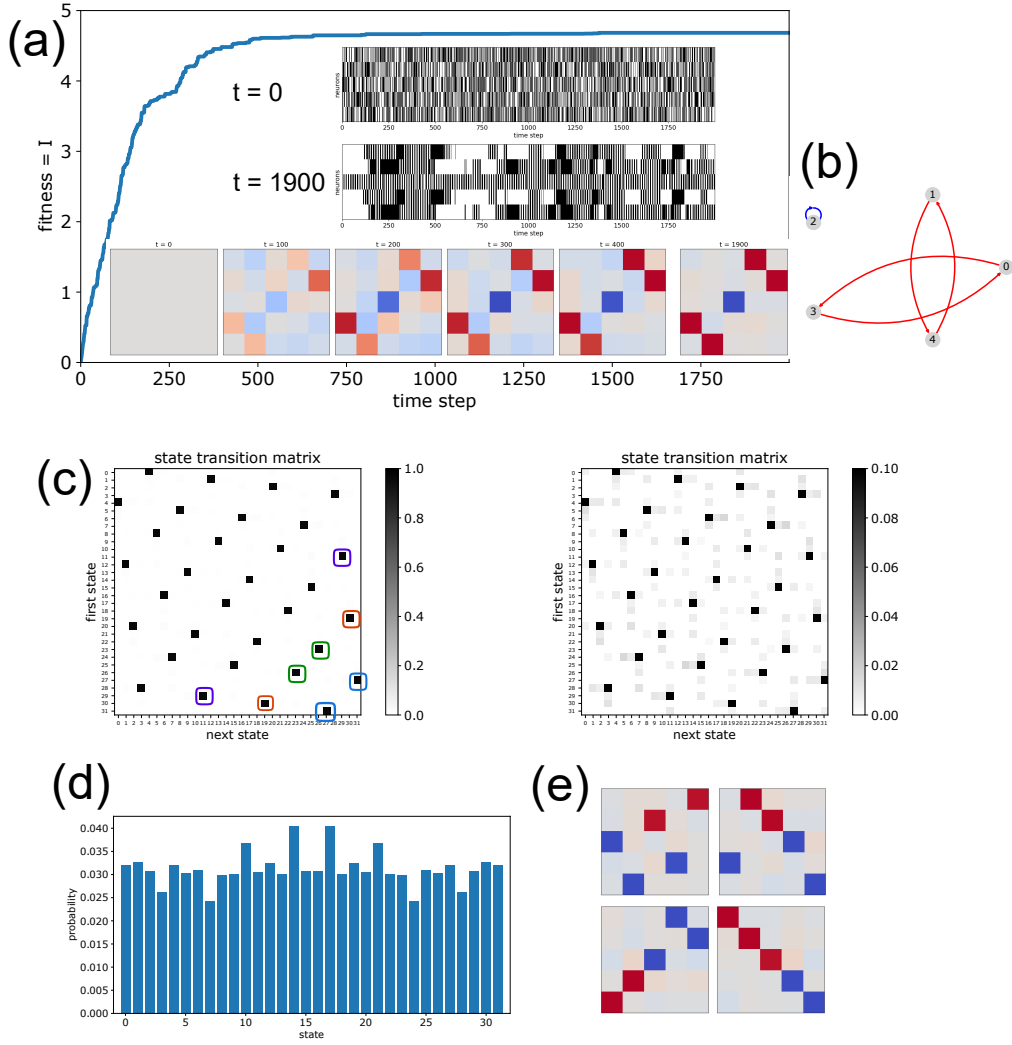


Figure 3: **Evolutionary optimization of state-to-state memory in a SBM with $N = 5$ neurons.** (a) Mutual Information $I[\vec{x}(t), \vec{x}(t+1)]$ grows monotonically with the evolutionary time step t (blue curve). Starting from a weight matrix with all elements zero (lower inset, left matrix), a pattern emerges with four strongly positive weights (red) and one strongly negative weights (blue). While neurons produce independent random walks for $t=0$ (upper inset), the system shows a multi-attractor dynamics at the final time step $t=1900$ (middle inset). (b) Network representation of the evolved system, ignoring small background matrix elements. (c) Transition probabilities between the 32 global states of the system (left matrix). Each state (matrix rows) has only one dominant successor state (matrix columns), leading to a highly predictable dynamics. In particular, pairs of states form 2-cycles as unstable attractors (three of the 2-cycles are marked by colors). A closer look at the smaller matrix elements (right matrix) reveals that each state also has several low-probability successor states, allowing for a switching between the attractors. (d) The 32 global states are visited with comparable probability, thus maximizing the entropy of the system. (e) Four independently optimized weight matrices. As a general rule, there emerge only $N=5$ matrix elements with large positive (red) or negative (blue) values, arranged such that they do not share the same rows or columns (Subsequently called the 'N-rooks principle'). Note that the individual strength of the matrix elements was limited to $|w_{ij}| < 5$ in the evolutionary optimization. Without this restriction, the life-time of the cyclic attractors becomes arbitrarily long and switching between them happens only extremely infrequently.

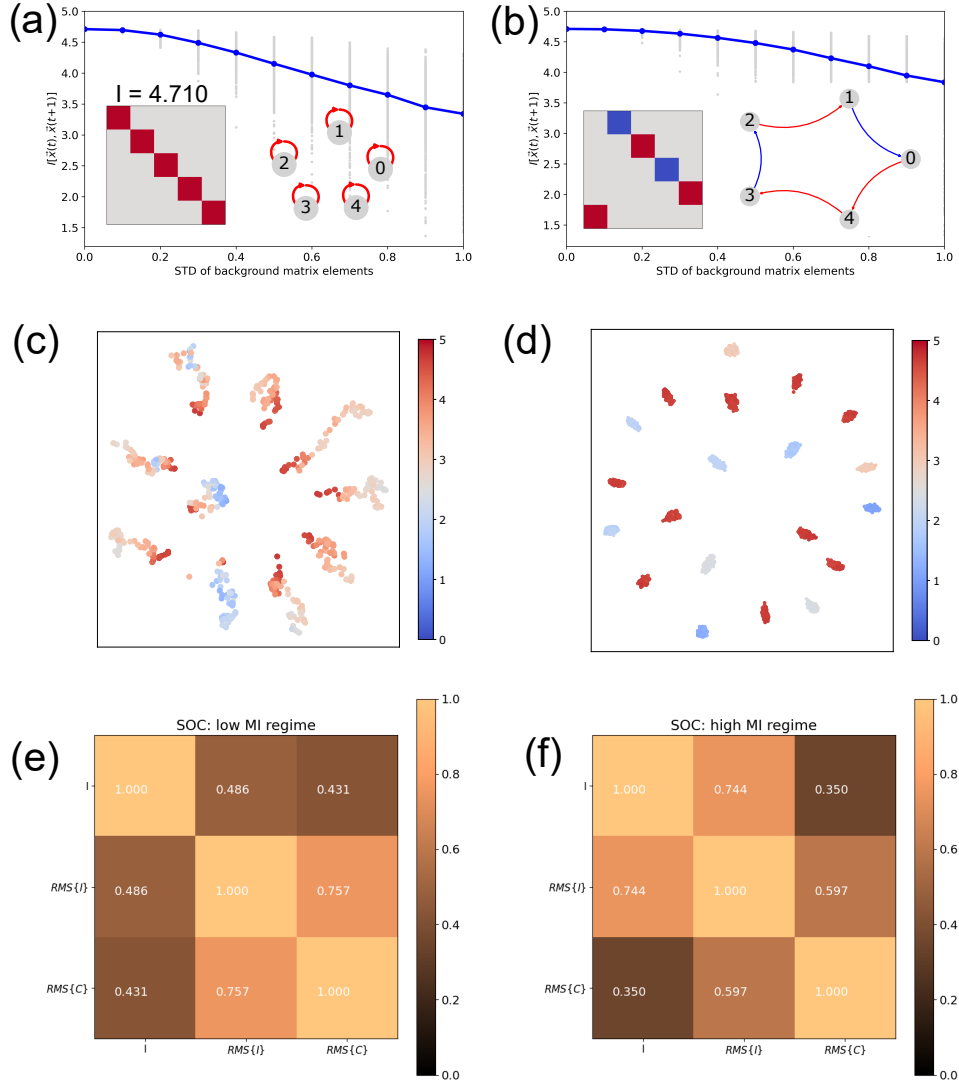


Figure 4: Exploring networks with high state-to-state memory. (a,b) Reverse engineering the weight matrices evolved in Fig.3 revealed a general pattern called the N-rooks principle. Such matrices can therefore be constructed from the scratch by accordingly placing N large positive or negative matrix elements $|w_{ij}| = 5$ into a $N \times N$ zero matrix. We find that all such N-rooks matrices have the same maximal mutual information $I = I[\vec{x}(t), \vec{x}(t+1)] = 4.710$. Two examples are shown as insets, both as weight matrix and as network graph. If the remaining $N^2 - N$ matrix elements are filled up with normally distributed random numbers of increasing standard deviation, the mutual information is degrading on average (blue curves, statistical fluctuations shown in gray). (c) To demonstrate that the N-rooks matrices are local maxima of mutual information in the N^2 -dimensional weight matrix space, we start from ten perfect N-rooks matrices (red) and then diffuse away from these points by iteratively adding small random numbers to the matrix elements. The plot shows a two-dimensional MDS visualization of the resulting diffusive random walks, with the mutual information color coded. (d) We next produce a larger test set of weight matrices with high mutual information by generating a cluster of random variants around each perfect 'central' N-rook matrix with a restricted distance to the cluster center (dark red spots). If now the positions of the large elements in the ten N-rook matrices are randomly shuffled and variants are again generated from the resulting 'non-N-rooks' matrices, we obtain a control set of matrices with smaller mutual information (weak red and weak blue spots), but with the same statistical distribution of weights. (e,f) The test set of high-MI matrices and the control set of lower-MI matrices is used to assess the similarity between the three measures of state-to-state memory, based on the SOC measure. We find again a reasonable agreement of $SOC = 0.757$ between the pairwise measures $RMS\{I\}$ and $RMS\{C\}$ in the low-MI control set (e), but this agreement is lost in the high-MI test set (f). Surprisingly, the pairwise $RMS\{I\}$ approximates the full I with $SOC = 0.744$ in this high-MI regime.

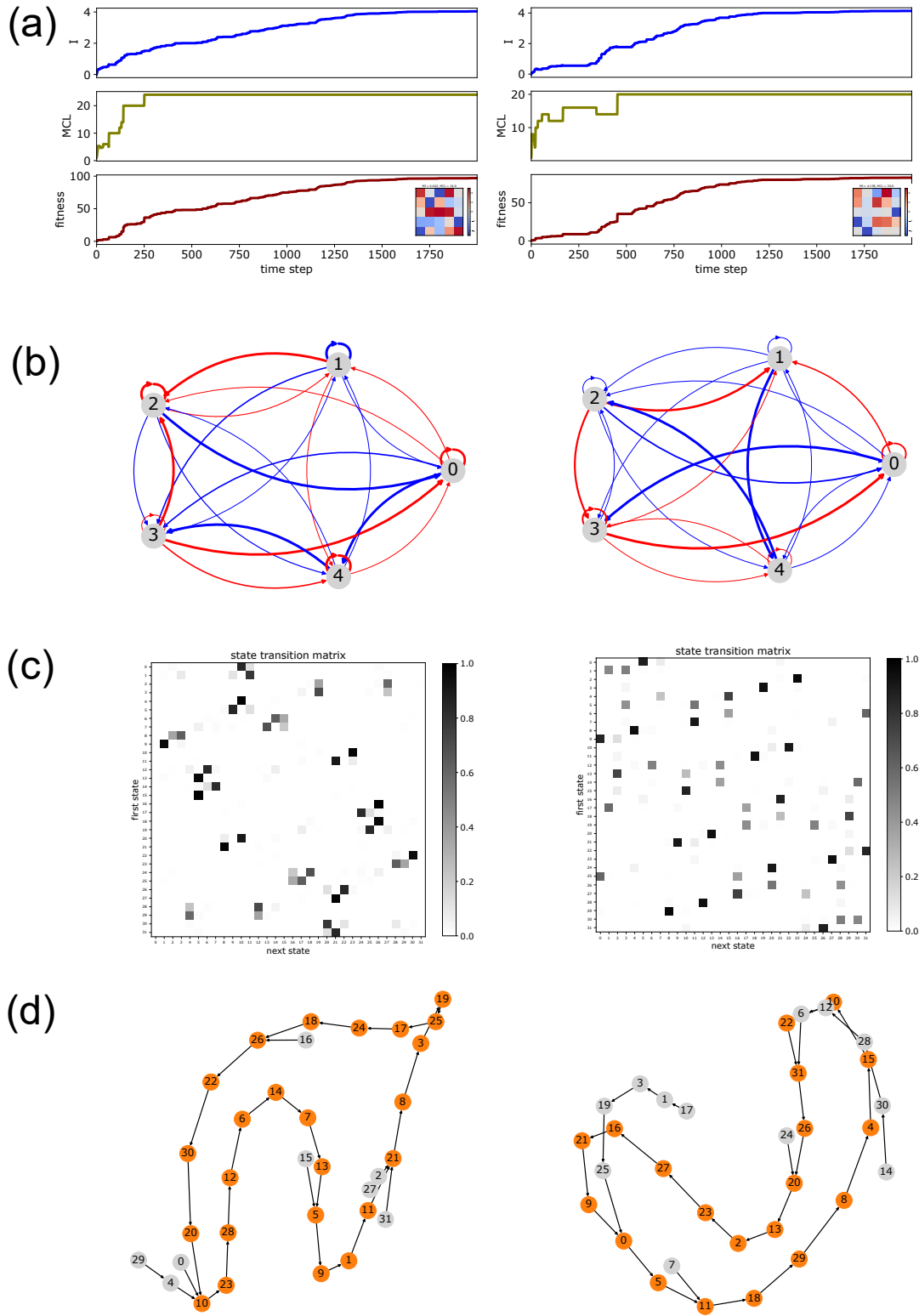


Figure 5: **Simultaneous optimization of state-to-state memory I and mean cycle length (MCL) of periodic attractors**, demonstrated in two independent evolutionary runs (left and right column). (a) The fitness (red), defined as the product $I \times \text{MCL}$, is increasing monotonously. The individual optimization factors (blue and olive) show an overall growth to larger values, but they also drop temporarily. (b) The resulting evolved networks do not follow the N-rooks principle any longer, and as a result the state-to-state memory is large but sub-optimal ($I = 4.042$ in the left and $I = 4.138$ in the right example). (c) The state transition matrices are not as sparse as in the case of N-rooks networks, so that each global system state can randomly switch between several successor states. (d) Nevertheless, there exists one dominating path through state space in the form of a single long cyclic attractor (consisting of 24 states in the left and 20 states in the right example). Note that states belonging to the cyclic attractor itself are colored in orange, transient states in gray.